J Therm Anal Calorim (2011) 104:343–349
DOI 10.1007/s10973-010-1067-3

Calorimetric studies on an insect antifreeze protein ApAFP752 from *Anatolica polita*

Xinfang Mao · Zhongyuan Liu · Honglei Li · Ji Ma · Fuchun Zhang

Received: 6 July 2010 / Accepted: 16 September 2010 / Published online: 8 October 2010

Abstract Many ectotherms organisms produce antifreeze proteins (AFPs), also known as thermal hysteresis proteins (THPs), which can lower the freezing temperature of body liquids without significantly affecting the melting point. In this article, thermal hysteresis activity (THA) of ApAFP752 from the desert beetle *Anatolica polita* was measured with differential scanning calorimetry (DSC). When the ice fraction was less than 25.3%, a delay in the onset temperature of refreezing was observed, indicating that the ApAFP752 solution has thermal hysteresis effect. When the amount of ice in the solution was less than 5.1%, THA of the ApAFP752 reached as high as 0.76 °C. THA of ApAFP752 was concentration-dependent. Hydrophilic ability of ApAFP752 was evaluated by thermal gravimetry (TG). The results of TG showed that ApAFP752 has strong hydrophilicity. The secondary structure of ApAFP752 was studied with circular dichroism (CD). The CD spectrum from 190 to 240 nm indicated a well-defined secondary structure consisting of 11.1% α-helix, 53.6% β-sheet, 8.3% turn, and 27.0% random coil.

Keywords Antifreeze protein · Thermal hysteresis activity · Differential scanning calorimetry · Thermal gravimetric analysis · Circular dichroism

Abbreviations

THA	Thermal hysteresis activity
BSA	Bovine serum albumin
IPTG	Isopropyl-l-thio-β-D-galactopyranoside
SDS-PAGE	Sodium dodecyl sulfate-polyacrylamide gel electrophoresis
CD	Circular dichroism

Introduction

The production of antifreeze proteins (AFPs) is an adaptive response of some ectotherms to cold environments, which allow them to survive subzero temperatures by inhibiting ice growth [1–5]. AFPs non-colligatively produce a temperature difference between the freezing point (T_f) and the melting point (T_m) of the body fluid, termed thermal hysteresis activity (THA), i.e., THA $= T_m - T_f$ [6, 7]. This feature enables the use of AFPs in cryopreservation of cells, tissues, as well as food products [8–11].

Analyses of the crystal structures of AFPs from various species have revealed that they typically display a flat hydrophilic side with oxygen atoms in the ice lattice, through which they are considered to directly interact with one or more planes of a growing ice crystal. The ice lattice mimicry found in most AFPs is considered essential for their ice-binding function [12–14].

X. Mao · Z. Liu · J. Ma (✉) · F. Zhang (✉)
Xinjiang Key Laboratory of Biological Resources and Genetic Engineering, College of Life Science and Technology, Xinjiang University, Urumqi 830046, China
e-mail: majibrge@yahoo.cn

F. Zhang
e-mail: zfcxju@gmail.com

X. Mao
e-mail: lzy1168@gmail.com

Z. Liu
e-mail: lilyxjmm@163.com

H. Li
School of Medicine, Tsinghua University, Hai'dian District, Beijing 100084, China
e-mail: lihongleihn@163.com

The beetle *Anatolica polita* (Coleoptera: Tenebrionidae) is distributed throughout Gurbantonggut Desert in Xinjiang and Central Asia, where the difference in temperature between summer and winter and day and night in summers varies much. These hostile environments may suggest that AFPs (ApAFP) in *A. polita* could have high THA. A recombinant protein ApAFP752 from beetle *A. polita* was obtained in a soluble form. The predicted three-dimensional structure of ApAFP752 was a right-handed parallel β-helix consisting of six repetitive 12-amino acid loops. The consensus sequence for these repeated loops was TCT/IXSXXCXXAX, where X stands for any amino acids, as described previously [12]. This sheet contained the array of threonine residues from the TCT/I motif that may be the putative ice-binding face [14, 15].

THA value is commonly measured with direct microscopic observation of crystal growth in a sample by employing a nanoliter osmometer [16, 17]. Another method is calculated approximately by the freezing point measurements by using a Micro-Osmometer [18]. Although microscope techniques that permit direct observation of the melting and growth of ice crystals have most often been used to measure THA values, differential scanning calorimetry (DSC) has been extensively used to study ice formation in biological samples, and DSC also provides an accurate method to analyze the TH activity of AFPs [7, 19–23]. DSC could monitor the thermal response of a sample to temperature changes, or isothermally [24]. At the same time, the exothermic and endothermic events during state changes of the sample can be monitored. The same temperature program is applied to a sample and a reference pan, and the difference in heat flow to each pan is measured. The transitions appear as endothermic peaks if heat is absorbed as ice melted or as exothermic peaks if heat is given out as ice formed.

Thermal gravimetry (TG) is a well-established set of techniques for obtaining qualitative and quantitative information about the effects of various heat treatments on materials of all kinds. This technique involves monitoring the mass loss of the sample in a chosen atmosphere (usually nitrogen or air) as a function of temperature [25]. TG is inherently quantitative and, therefore, an extremely powerful thermal technique, but gives no direct chemical information [26, 27].

To see whether there are differences in thermal behavior between the control BSA and ApAFP752, DSC and TG measurements were performed in this study. The aim of this article is to accurately investigate TH activity of ApAFP752 with DSC and to study the hydrophilicity of ApAFP752 by TG method. Subsequently, to understand the mechanism of thermal behavior of ApAFP752, the structural information of ApAFP752 at its natural state was obtained with CD spectrum.

Experimental

Materials

ApAFP752 was produced by *Escherichia coli* BL21 (DE3) strain containing plasmid pET32a-*Apafp752* (*Apafp752* GenBank no. GU358703) with 0.8 mM IPTG induction. As expected, SDS-PAGE analysis showed that recombinant ApAFP752 was highly expressed in *E. coli* BL21 (DE3) and the soluble component was obtained. High quality ApAFP752 was yielded with Ni-NTA affinity, anion exchange, and gel filtration chromatography. Purified recombinant protein ApAFP752 was identified by SDS-PAGE and Western blotting.

The molecular size of this recombinant ApAFP752 was determined to be 30 kDa. The concentration of the protein was 1 mg mL^{-1} for DSC and TG experiment. BSA was purchased from AMRESCO Chemical (USA) and the concentration was 3 mg mL^{-1}. Samples were all dissolved in 10 mM phosphate buffer, pH 7.4 (PBS). Water was double distilled.

DSC

A DSC Q2000 (TA Instruments, USA) was used in this study. Empty aluminum hermitric pans were used for baseline calibration. BSA solution was used as a control to make a comparison between solutions with and without ApAFP752. About 5 μL of sample was placed in an aluminum pan. The mass of the sample was recorded using an analytical balance. The TH activity of AFP was measured by DSC as described in detail elsewhere [20, 21, 23]. Briefly, a sample was cooled to −30 °C (completely frozen), held at −30 °C for 10 min to allow the system to stabilize, and then slowly heated at a rate of 1 K min^{-1} to 10 °C. The melting point and the melt endothermic area (the enthalpy of melting) were recorded. The sample was then cooled at a rate of 1 K min^{-1} to −30 °C again, held at −30 °C for 10 min, and then slowly heated at the same rate to a hold temperature (T_h) at which the sample was not completely melted, containing a certain amount of ice crystal. To allow for ice–ApAFP752 interaction and system stabilization, the sample was held at this temperature for 5 min before being recooled at the same rate of 1 K min^{-1} to −30 °C. The onset temperature (T_o) of the crystallization and the refreeze exothermic area (the enthalpy of ice-inoculated freezing) were recorded.

The fraction of the ice (Nuclei (%)) in the sample was estimated as $[1 - (-\Delta H_r/\Delta H_m)] \times 100\%$, where ΔH_m is the enthalpy of melting and ΔH_r is the enthalpy of refreezing [23]. The experimental procedure above was repeated with different hold temperatures to obtain different partially melted systems with various ice-contents.

Scans at different T_h may result in different ice fractions in the sample, which may affect the measured THA [20, 28]. The difference between the T_h and the T_o, THA = $T_h - T_o$, is usually represented as the THA determined using the DSC method to quantitatively assess the THA at various ice fractions [20, 29].

TG analysis

The hydrophilicity of the samples was assayed by a TG method, which reflected the hydrophilic affinity of the samples [30]. The TG analyzer was heated from 25 to 150 °C at a rate of 15 K min^{-1} with a nitrogen flow of 25 mL min^{-1} by TGA Q5000 (TA Instruments, USA). Aliquots of 20 μL of sample [PBS, BSA, and ApAFP752, respectively] were loaded into platinum pans. PBS was used as the control. The TG curve showed mass loss during the heating process.

Circular dichroism (CD) spectrum

CD spectra were measured from 190 to 250 nm on J-715 (JASCO, Japan). Sample was dissolved in PBS (pH 7.4) at a concentration of 3 μmoL L^{-1}, and placed in a 0.1 cm path length quartz cuvette. Baseline calibration was made against the sample. Spectrum was recorded with a scan speed of 50 nm min^{-1}. Data obtained from CD spectroscopy were converted into molar ellipticities (deg cm^2 $dmol^{-1}$), and used for secondary structure analysis by using Jasco Jwsse 32 secondary structure estimation software. Wavelength scan data were collected every 1 nm with a 3 s data averaging time, and three scans were averaged.

Results

DSC measurements

DSC curves of refreezing (1 K min^{-1}) of partially melted BSA solution are presented in Fig. 1 and data are given in Table 1. Frozen BSA was heated to cause partial melting at different hold temperature. The sample was then cooled and recrystallized. The area under the exothermic curves increased with the increase of T_h from −1.8 (a), −1.7 (b), −1.5 (c), −1.3 (d) to −1.1 °C (e), indicating that the amount of ice nuclei in the equilibrium sample decreased accordingly. Recrystallization of the melted part started immediately after the temperature dropped, and the exothermic peak appeared without any delay. The result indicated that the BSA solution had no thermal hysteresis effect. When T_h rised to −0.9 °C, complete melting of the frozen BSA solution was observed, and the solution refreezed at the supercooling point of −13.93 °C.

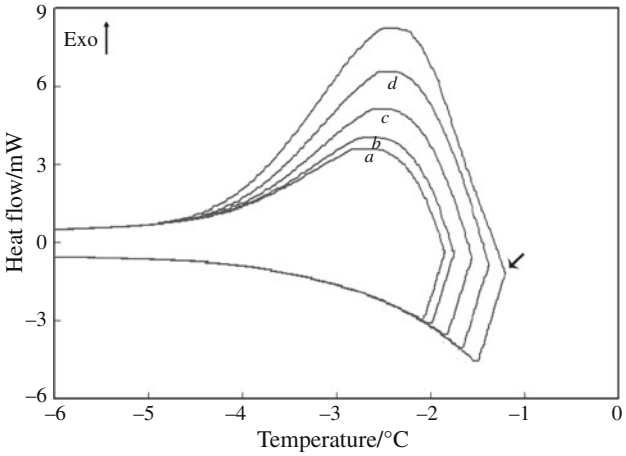

Fig. 1 DSC curves of refreezing (1 K min^{-1}) of partially melted BSA. The hold temperature (T_h) of the curves from a to e are −1.8, −1.7, −1.5, −1.3, and −1.1 °C, respectively. No delay in the onset temperature has been shown with an *arrow*

Table 1 The hold and onset temperature (T_h and T_o), recrystallization enthalpy, ice fraction, and THA of BSA (3 mg mL^{-1})

T_h/°C	−1.8	−1.7	−1.5	−1.3	−1.1	−0.9
T_o/°C	−1.81	−1.71	−1.53	−1.33	−1.12	−13.93
ΔH_r/ J g^{-1}	−143.3	−180.0	−225.4	−256.2	−273.7	−260.6
Nuclei "%"	51.0	38.5	23.0	12.5	6.5	0
THA/ °C	0.01	0.01	0.03	0.03	0.02	

Melting enthalpy ΔH_m = 292.7 J g^{-1}

Nuclei (%) = $[1 - (-\Delta H_r)/\Delta H_m] \times 100\%$

DSC curves and corresponding data of the recrystallization of partially melted ApAFP752 solution are presented in Fig. 2 and Table 2. Similarly, there was a decrease in the ice fraction with increasing of T_h from −1.9 to −0.9 °C. As T_h was −1.9 (a), −1.8 (b), −1.7 (c), −1.6 (d), and −1.5 °C (e) and the ice fraction was more than 25.3%, the recrystallization of partially melted ApAFP752, very much like BSA, started without any delay as the temperature dropped, and the freezing peaks appeared immediately. When the ice fraction was less than 25.3%, however, a delay in the onset temperature of refreezing was observed to increase from 0.3 to 0.76 °C as T_h increased from −1.4 (f) to −0.9 °C (k). This indicated that the ApAFP752 solution has thermal hysteresis effect. When T_h rised to −0.8 °C, the frozen ApAFP752 solution was completely melted, and then with the temperature dropped the solution refreezed at the supercooling point of −12.36 °C.

Figure 3 shows the concentration dependence of the TH activity of ApAFP752 measured at cooling rate of 1 K min^{-1}. At 0.1, 0.3, 0.5, and 1.0 mg mL^{-1} ApAFP752,

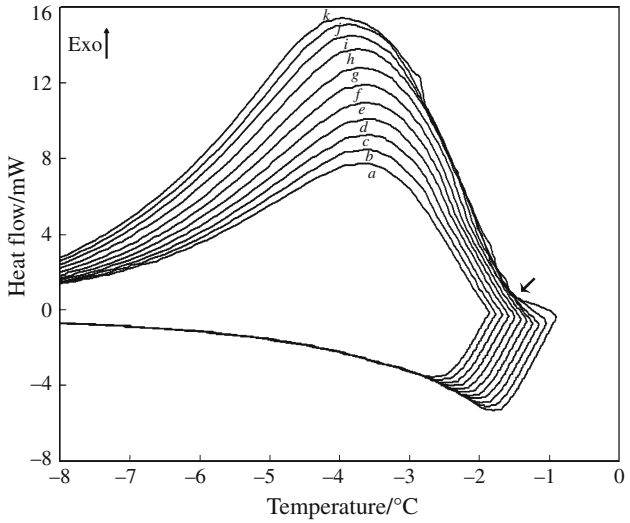

Fig. 2 DSC curves of refreezing (1 K min^{-1}) of partially melted ApAFP752. The hold temperature (T_h) of the curves from *a* to *k* are −1.9, −1.8, −1.7, −1.6, −1.5, −1.4, −1.3, −1.2, −1.1, −1.0, and −0.9 °C, respectively. No thermal hysteresis effect was observed in curves *a*, *b*, *c*, *d*, and *e*, whereas, THA of 0.3, 0.38, 0.45, 0.67, 0.69, and 0.76 °C was observed in curves from *f* to *k*, respectively. The delay in the onset temperature is shown with an *arrow*

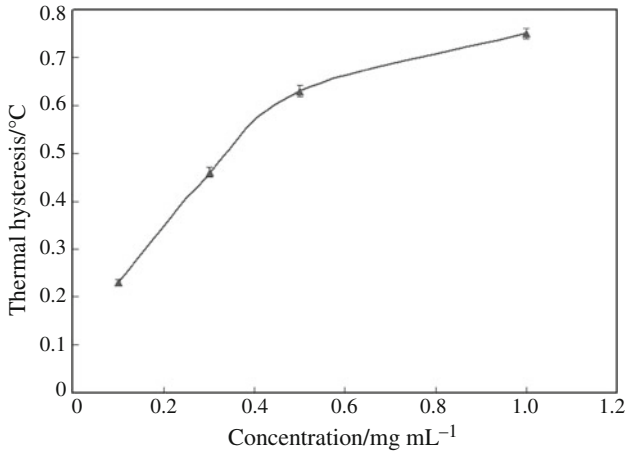

Fig. 3 Concentration dependence of THA for ApAFP752. The concentration of ApAFP752 is 0.1, 0.3, 0.5, and 1.0 mg mL^{-1}, respectively. Each point represents the mean of three experiments and the *error bar* represents the standard deviation

the TH activity was 0.23, 0.46, 0.63, and 0.76 °C, respectively (Table 3). There was an increase in TH activity with the increase of concentration from 0.1 to 1.0 mg mL^{-1}, indicating that the TH activity of ApAFP752 was concentration-dependent.

Thermo gravimetric analysis

Hydrophilic ability of ApAFP752 was evaluated by TG. As shown in Fig. 4, from left to right, the curves were PBS, BSA, 1 mg mL^{-1} ApAFP752, and 3 mg mL^{-1} ApAFP752, respectively. It indicated that there was different mass remaining at the same temperature. The exact temperature of 90% sample mass loss was monitored in Table 3. The temperatures were 114.51, 115.12, 119.86, and 120.61 °C for PBS, BSA, ApAFP752 (1 mg mL^{-1}), and ApAFP752 (3 mg mL^{-1}) solutions, respectively, when the mass loss was 90%. The ApAFP752 had higher temperature for 90% mass loss than those of PBS and BSA solutions. Therefore, the water of ApAFP752 cost more time to escape from the protein solution than that of PBS and BSA solutions. The result suggested that ApAFP752 has higher hydrophilicity than BSA. ApAFP752 (3 mg mL^{-1}) had higher temperature for 90% mass loss than those of ApAFP752 (1 mg mL^{-1}) solution, indicating that hydrophilic ability of ApAFP752 was also concentration-dependent.

The water evaporation of PBS, BSA, ApAFP752 (1 mg mL^{-1}), and ApAFP752 (3 mg mL^{-1}) solutions stopped at about 122.02, 124.37, 127.39, and 129.45 °C, respectively (Table 4). It indicated that the water of ApAFP752 solution takes more time to evaporate because of the strong hydrophilicity of ApAFP752.

CD measurement

Secondary structure provides useful information for understanding the functional mechanism of the ApAFP752. The CD spectrum of ApAFP752 incubated at room temperature showed a single maximum negative ellipticity between 210 and 220 nm (Fig. 5), indicating formation of a β-sheet structure [31, 32]. A mixed secondary structure of

Table 2 The hold and onset temperature (T_h and T_o), recrystallization enthalpy, ice fraction, and THA of ApAFP752 (1 mg mL^{-1})

T_h/°C	−1.9	−1.8	−1.7	−1.6	−1.5	−1.4	−1.3	−1.2	−1.1	−1.0	−0.9	−0.8
T_o/°C	−1.92	−1.83	−1.73	−1.62	−1.54	−1.70	−1.68	−1.65	−1.77	−1.69	−1.66	−12.36
ΔH_r/J g^{-1}	−142.7	−168.4	−183.0	−198.3	−224.2	−265.1	−276.8	−309.5	−324.2	330.5	−336.8	−345.6
Nuclei "%"	59.8	52.6	48.4	44.1	36.8	25.3	22.0	12.8	8.7	6.9	5.1	0
THA/°C	0.02	0.03	0.03	0.02	0.04	0.3	0.38	0.45	0.67	0.69	0.76	

Melting enthalpy $\Delta H_m = 354.9$ J g^{-1}

Nuclei (%) = $[1 - (-\Delta H_r)/\Delta H_m] \times 100\%$

Table 3 The hold and onset temperature (T_h and T_o), melting enthalpy, recrystallization enthalpy, ice fraction, and THA of ApAFP752 with different concentrations

Samples	T_h/°C	T_o/°C	ΔH_m/J g^{-1}	ΔH_r/J g^{-1}	Nuclei "%"	THA/°C
ApAFP752 "0.1 mg mL^{-1}"	−1.0	−1.23	254.7	−241.9	5.0	0.23[a]
ApAFP752 "0.3 mg mL^{-1}"	−1.0	−1.46	277.9	−261.8	5.8	0.46[b]
ApAFP752 "0.5 mg mL^{-1}"	−0.9	−1.53	300.6	−281.9	6.2	0.63[c]
ApAFP752 "1 mg mL^{-1}"	−0.9	−1.66	354.9	−336.8	5.1	0.76[d]

Different *lower case letters* indicate significant differences ($p < 0.01$). Values are means ± SD of three replicates

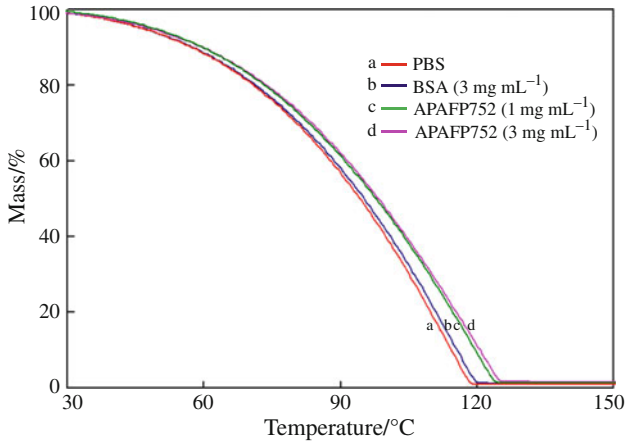

Fig. 4 TG curves of PBS, BSA (3 mg mL^{-1}), ApAFP752 (1 mg mL^{-1}), and ApAFP752 (3 mg mL^{-1})

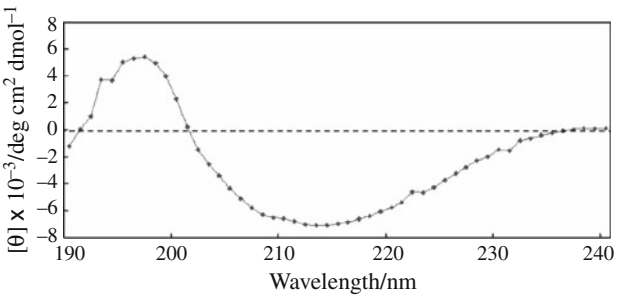

Fig. 5 The CD spectrum of the ApAFP752 in PBS, pH 7.4 at room temperature

11.1% α-helix, 53.6% β-sheet, 8.3% turn, and 27.0% random coils was deduced. The β-sheet structure is the predominant secondary structure of the ApAFP752.

Discussion

TH activity of AFP was determined usually using the DSC method at various ice fractions [20, 22]. As shown in Fig. 1, in an equilibrium solution absent of ApAFP752, the formation of an ice nucleus and further crystallization occur almost at the same time as the temperature drops. When in the presence of ApAFP752, the ice–ApAFP752 interaction results in a delay in crystallization until the temperature is low enough to overcome the effect of ApAFP752 (Fig. 2).

Figure 2 clearly showed that when large amount of ice (>25.3%) existed in the system, the level of ApAFP752 accumulation was not high enough to suppress the ice growth as the temperature dropped. Explosive crystallization and the drop of temperature, therefore, were synchronistic. When the sample contained less ice (≤25.3%), the freezing point of the partially melted ApAFP752 solution was considerably lowered. The THA of ApAFP752 solution was increased from 0.3 to 0.76 °C when the ice fraction was decreased, which is similar to that found in DAFP-1 sample [23]. This condition is much closer to the initial natural phase when insect *A. polita* meet severe weather and start to freeze in the wild. Higher THA was observed with smaller ice fraction (5.1%) in the solution of ApAFP752. This result was also in agreement with the proposed mechanism for AFP function [4, 33].

According to TG data, the water of the ApAFP752 solution takes more time to evaporate than the control because of the strong hydrophilicity of ApAFP752, similar to that of other known AFPs [34, 35]. ApAFP752 was

Table 4 Total mass loss of PBS, BSA, and ApAFP752 by TG

Samples	Heating rate/K min^{-1}	90% weight loss/°C	Evaporation stop/°C
PBS	15	114.51 ± 0.12[a]	122.02 ± 0.18[a]
BSA "3 mg mL^{-1}"	15	115.12 ± 0.14[a]	124.37 ± 0.18[b]
ApAFP752 "1 mg mL^{-1}"	15	119.86 ± 0.11[b]	127.39 ± 0.12[c]
ApAFP752 "3 mg mL^{-1}"	15	120.61 ± 0.16[c]	129.45 ± 0.20[d]

Different *lower case letters* indicate significant differences ($p < 0.01$). Values are means ± SD of three replicates

composed of 78.8% hydrophilic amino acids, contributing to the strong hydrophilic ability structurally. The strong hydrophilicity of ApAFP752 confers its ability to convert the free water to binding water in the beetle body liquid, which is significantly important for its adaptation to the water-deficit caused by extreme environment conditions: drought and freezing.

Secondary structure provides the most useful information for understanding the real mechanism of *A. polita* AFP. CD technique is based on the differential absorption of left- and right-circularly polarized light by optically active molecules [36]. It has been widely used to study protein secondary structure conformations (β-sheet, α-helix, etc.) in the far-UV range, where the peptide bonds are the main chromophore and absorb at wavelengths below 240 nm [37]. CD spectral studies demonstrated that the predominant secondary structure of ApAFP752 was β-sheet (Fig. 5). It is similar to that of TmAFP from *Tenebrio molitor* possessing right-handed β-helix [32]. The predicted 3D structure shows that most hydrophilic amino acid residues of the ApAFP752 located on the faces of the β-sheet (data not shown). How does this structure actually function is still under investigation.

Acknowledgements This study was supported by a Grant (No. 30760056 and 200991130) from National Natural Science Foundation of China, the Open Fund from Xinjiang Key Laboratory of Biological Resources and Genetic Engineering (No. XJDX0201-200904) and the Scientific Foundation of Zoology in Xinjiang University.

References

1. Knight CA, Cheng CC, De Vries AL. Adsorption of α-helical antifreeze peptides on specific ice crystal surface planes. Biophys J. 1991;59:409–18.
2. Sidebottom C, Buckley S, Pudney P, Twigg S, Jarman C, Holt C, Telford J, McArthu A, Worrall D, Hubbard R, Lillford P. Heat-stable antifreeze protein from grass. Nature. 2000;406:256.
3. Graham LA, Davies PL. Glycine-rich antifreeze proteins from snow fleas. Science. 2005;310:461.
4. Wierzbicki A, Dalal P, Cheatham TE, Knickelbein JE, Haymet ADJ, Madura JD. Antifreeze proteins at the ice/water interface: three calculated discriminating properties for orientation of type I proteins. Biophys J. 2007;93:1442–51.
5. Li N, Chibber BAK, Castellino FJ, Duman JG. Mapping of disulfide bridges in antifreeze proteins from overwintering larvae of the beetle *Dendroidesc anadensis*. Biochemistry. 1998;37:6343–50.
6. Feeney RE, Hofmann R. Depression of freezing point by glycoproteins from an Antarctic fish. Nature. 1973;243:357–9.
7. Wang S, Amornwittawat N, Juwita V, Kao Y, Duman JG, Pascal TA, Goddard WA, Wen X. Arginine, a key residue for the enhancing ability of an antifreeze protein of the Beetle *Dendroides canadensis*. Biochemistry. 2009;48:9696–703.
8. Fletcher GL, Goddard SV, Wu Y. Antifreeze proteins and their genes: from basic research to business opportunity. Chemtech. 1999;30:17–28.
9. Venketesh S, Dayananda C. Properties, potentials, and prospects of antifreeze proteins. Crit Rev Biotechnol. 2008;28:57–82.
10. Yeh CM, Kao BY, Peng HJ. Production of a recombinant type 1 antifreeze protein analogue by *L. lactis* and its applications on frozen meat and frozen dough. J Agric Food Chem. 2009;57:6216–23.
11. Zhang C, Zhang H, Wang L. Effect of carrot (*Daucus carota*) antifreeze proteins on the fermentation capacity of frozen dough. Food Res Int. 2007;40:763–9.
12. Liou YC, Tocilj A, Davies P, Jia ZC. Mimicry of ice structure by surface hydroxyls and water of a β-helix antifreeze protein. Nature. 2000;406:322–4.
13. Marshall CB, Daley ME, Sykes BD, Davies PL. Enhancing the activity of a β-helical antifreeze protein by the engineered addition of coils. Biochemistry. 2004;43:11637–46.
14. Graether SP, Kuiper MJ, Gagne SM, Walker VK, Jia ZC, Sykes BD. Davies PL. β-Helix structure and ice-binding properties of a hyperactive antifreeze protein from an insect. Nature. 2000;406:325–8.
15. Jia ZC, Davies PL. Antifreeze proteins: an unusual receptor–ligand interaction. Trends Biochem Sci. 2002;27:101–6.
16. Nicodemus J, O'Tousa JE, Duman JG. Expression of a beetle, *Dendroides canadensis*, antifreeze protein in *Drosophila melanogaster*. J Insect Physiol. 2006;52:888–96.
17. Lin X, O'Tousa JE, Duman JG. Expression of two self-enhancing antifreeze proteins from the beetle *Dendroides canadensis* in *Drosophila melanogaster*. J Insect Physiol. 2010;56:341–9.
18. Qiu LM, Ma J, Wang J, Zhang FC, Wang Y. Thermal stability properties of an antifreeze protein from the desert beetle *Microdera punctipennis*. Cryobiology. 2010;60:192–7.
19. Hansen TN, Baust JG. Differential scanning calorimetric analysis of antifreeze protein activity in the common mealworm, *Tenebrio molitor*. Biochim Biophys Acta. 1988;957:217–21.
20. Lu M, Wang B, Li Z, Fei Y, Wei L, Gao Sh. Differential scanning calorimetric and circular dichroistic studies on plant antifreeze proteins. J Therm Anal Calorim. 2002;67:689–98.
21. Ramlov H, De Vries AL, Wilson PW. Antifreeze glycoproteins from the Antarctic fish *Dissostichus mawsoni* studied by differential scanning calorimetry (DSC) in combination with nanolitre osmometry. Cryo Lett. 2005;26:73–84.
22. Hansen TN, De Vries AL, Baust JG. Calorimetric analysis of antifreeze glycoproteins of the polar fish, *Dissostichus mawsoni*. Biochim Biophys Acta. 1991;1079:169–73.
23. Amornwittawat N, Wang S, Duman JG, Wen X. Polycarboxylates enhance beetle antifreeze protein activity. Biochim Biophy Acta. 2008;1784:1942–8.
24. Thelma M, Virginia CA, Ana M. Thermal behavior of in vitro mineralized anionic collagen matrices. J Therm Anal Calorim. 2009;95:945–9.
25. Vijayasundaram V, Ramasamy V, Palaniappan PLRM. The study of the changes in the thermal properties of *Labeo rohita* bones due to arsenic exposure. J Therm Anal Calorim. 2009;98:183–8.
26. Sohar G, Pallagi E, Szabo-Revesz P, Toth K. New thermogravimetric protocol for the investigation of normal and damaged human hyaline cartilage. J Therm Anal Calorim. 2007;89:853–6.
27. Öz S, Kurtaran R, Arıcı C, Ergun Ü, Dinçer Kaya FN, Emregül KC, Atakol O, Ülkü D. Two non-linear azide containing heteronuclear complexes: crystal structure and thermal decomposition. J Therm Anal Calorim. 2010;99:363–8.
28. Verdu JR, Casas JL, Lobo JM, Numa C. Dung beetles eat acorns to increase their ovarian development and thermal tolerance. PLoS ONE. 2010;5:1–8.
29. Zhang C, Zhang H, Wang L, Yao HY. Validation of antifreeze properties of glutathione based on its thermodynamic characteristics and protection of baker's yeast during cryopreservation. J Agric Food Chem. 2007;55:4698–703.
30. Zhang C, Zhang H, Wang L, Zhang JH, Yao HY. Purification of antifreeze protein from wheat bran (*Triticum aestivun* L.) based

on its hydrophilicity and ice-binding capacity. J Agric Food Chem. 2007;55:7654–8.
31. Li N, Kendric BS, Manning MC, Carpenter JF, Duman JG. Secondary structure of antifreeze proteins from overwintering larvae of the beetle *Dendroides canadensi*s. Arch Biochem Biophys. 1998;360:25–32.
32. Sieber V, Jurnak F, Moe GR. Circular dichroism of the parallel beta helical proteins pectate lyase C and E. Proteins. 1995;23:32–7.
33. Nishimiya Y, Kondo H, Takamichi M, Sugimoto H, Suzuki M, Miura A, Tsuda S. Crystal structure and mutational analysis of Ca^{2+}-independent type II antifreeze protein from Longsnout Poacher, *Brachyopsis rostratus*. J Mol Biol. 2008;382:734–46.
34. Graham LA, Liou YC, Walker VK, Davies PL. Hyperactive antifreeze protein from beetles. Nature. 1997;388:727–8.
35. Deng G, Andrews DW, Laursen RA. Amino acid sequence of a new type of antifreeze protein from the longhorn sculpin *Myoxocephalus octodecinspittosis*. FEBS Lett. 1997;402:17–20.
36. Dijk LV, Bobbert PA, Spano FC. Extreme sensitivity of circular dichroism to long-range excitonic couplings in helical supramolecular assemblies. J Phys Chem B. 2010;114:817–25.
37. Fiche JB, Laredo T, Tanchak O, Lipkowski J, Dutcher JR, Yada RY. Influence of an electric field on oriented films of DMPC/gramicidin bilayers: a circular dichroism study. Langmuir. 2010;26:1057–66.